Construction and Building Materials 119 (2016) 1–15

Contents lists available at ScienceDirect

Construction and Building Materials

journal homepage: www.elsevier.com/locate/conbuildmat

Axial compressive behavior of FRP-confined lightweight aggregate concrete: An experimental study and stress-strain relation model

Yingwu Zhou, Xiaoming Liu, Feng Xing, Hongzhi Cui, Lili Sui *

Guangdong Provincial Key Laboratory of Durability for Marine Civil Engineering, Shenzhen University, Shenzhen 518060, China

HIGHLIGHTS

- The paper presents an experimental study on FRP-confined LWAC.
- The aggregate type has a significant effect on the FRP-confined LWAC.
- The FRP confinement ratio has a great influence on the FRP-confined LWAC.
- Both the ultimate strength and strain model of FRP-confined LWAC are derived.
- A stress-strain model of FRP-confined LWAC is developed.

ARTICLE INFO

Article history:
Received 4 November 2015
Received in revised form 18 February 2016
Accepted 24 February 2016
Available online 12 May 2016

Keywords:
Carbon fiber-reinforced polymer
Lightweight aggregate concrete
Strength
Stress-strain relation
Confined concrete
Analytical modeling

ABSTRACT

Due to its low strength and high brittleness, lightweight aggregate concrete (LWAC) can mainly be used to fabricate non-load bearing structures. Wrapping LWAC with fiber-reinforced polymer (FRP) can effectively improve its mechanical properties, thereby allowing to realize a structural lightweight design. This study therefore aimed to investigate the effect of a FRP confinement on the mechanical properties of LWAC. Three types of coarse aggregate material, i.e., class 600 shale ceramsite, class 800 shale ceramsite and hollow sealed thin-wall steel balls, were selected to design the LWAC and compared in the experiments. After wrapping with three layers of FRP, the strengths of LWACs prepared from the three different materials were improved by a factor of 2.6, 2.1 and 5.4, respectively, whereas their ultimate deformations were improved by a factor of 33.4, 8.5 and 31.2, respectively. Meanwhile, the strength and stress-strain relation for the FRP-confined LWAC were obtained through axial compression tests. Models for the ultimate strength, the ultimate strain and the stress-strain relation of FRP-confined LWAC were successfully established, and a comparative analysis revealed that the predictions made using these models are very accurate. A numerical analysis of these models further showed that, for LWAC and normal concrete with the same strength and FRP confinement, the mechanical behavior was different and found to heavily depend on the FRP confinement aspect properties and the types of the light-weight aggregate.

1. Introduction

Lightweight aggregate concrete (LWAC) generally refers to concrete prepared from lightweight aggregate, ordinary sand (or lightweight sand), cement and water with a dry apparent density below or equal to 1950 kg/m^3 [1]. Compared with normal concrete of the same strength, the weight of LWAC is about 25∼30% lower. In addition to its lower weight, LWAC also offers a superior thermal-insulation, fire-resistance, sound-insulation and anti-seismic performance in comparison to normal concrete. However, the compressive strength, shearing strength and tensile strength of LWAC are relatively low. Its application potential is also restrained by its low elastic modulus, high creep and shrinkages, high brittleness and significantly lower ductility [2]. The strength and ductility of LWAC material significantly declines with decreasing density [3], and there is always a contradiction between strength and weight. Therefore, LWAC is mainly applied for the fabrication of boards, walls and other non-load bearing structures, and its application potential for the fabrication of columns, beams and other load-bearing structures is limited.

Fiber reinforced polymer (FRP) composites offer several advantages, e.g., a light weight, a high strength, a high corrosion resistance, and an excellent anti-fatigue performance, and can withstand acidic, alkaline, chloride and moist environments for long periods of time and can therefore extend the service life of

* Corresponding author.
E-mail address: suill8969@163.com (L. Sui).

http://dx.doi.org/10.1016/j.conbuildmat.2016.02.180
0950-0618/

structural materials beyond normal lifetimes. Confinement of concrete with FRP is a very effective way to improve the strength and ductility of concrete, and has been demonstrated in a large number of experiments. For instance, Jiang and Teng [4] investigated 48 concrete cylinder samples with a diameter of 152 mm, a height of 305 mm, and a strength of 33.1∼45.9 MPa and found that, when the test specimens were wrapped and confined with one, two, four, six or eight layers of FRP, the strength of the cylinders was improved by a factor of 1.39, 1.95, 2.89, 3.47 and 4.21, respectively. Ceteris paribus, the lower the initial strength of the concrete, the higher its strength improvement under FRP confinement. The circumferential confinement with FRP limits the lateral expansion of concrete under load, and the strength and deformation of the confined concrete are therefore significantly improved under triaxial compression [5], especially when large deformable FRP is used [6,7]. It can thus be inferred that confinement with FRP is also an effective method to solve the problems of the inadequate strength and the poor ductility of LWAC materials, which makes it a promising approach for realizing a structural lightweight design.

During the past decade, a variety of studies have been performed focusing on the effect of various parameters [4,5,8–20], e.g., the initial strength [4,5,8,9,17], the FRP thickness [4,5,8,17], the type of FRP material [4,5,8,10], the sectional shape [11–13], the sectional size [5], the initial deterioration damage [13–16], and the slenderness ratio [18], on the mechanical properties of FRP-confined normal concrete, and a number of strength [4,5,8,11,17,20,27] and stress-strain models [5,19–22,10,23–28] have been established. The results of these studies increased our understanding concerning the mechanical properties of FRP-confined normal concrete. However, these studies mainly focused on normal concrete, and, to the best of our knowledge, studies on FRP-confined LWAC columns have not been reported yet. Therefore, we aimed to investigate possibilities of improving the mechanical properties of LWAC based on a confinement with FRP.

In the present paper, the results of an experimental study and theoretical analysis of the mechanical properties of FRP-confined LWAC are reported. By measuring the mechanical properties of the LWAC before and after the confinement with FRP, the influence of the different types of coarse aggregate material and the number of FRP layers on the strength and deformation of the LWAC was investigated, and a stress-strain relation model were established for the FRP-confined LWAC. The obtained results therefore offer an experimental and theoretical framework for further studies on the mechanical properties of FRP strengthened LWAC structures.

2. Experimental programs

In this study, the axial compression test method was adopted to study the basic mechanical properties of FRP confined LWAC. In this section, the material and the test method are described in detail.

2.1. Test material and material properties

2.1.1. Preparation of the LWAC

Three types of LWAC were prepared and their mix proportions are provided in Table 1. For the preparation of the LWAC, P.II52.5R cement of Chinese standard and three different types of lightweight coarse aggregate were used as raw materials, i.e., continuously graded class 600 and class 800 crushed shale ceramsite with a diameter between 5 and 20 mm (Fig. 1a), and single-grade sealed thin-wall steel balls with a diameter of 20 mm (Fig. 1b). The main properties of the three different types of lightweight coarse aggregate are compared in Table 2. River sand with an apparent density of 2600 kg/m^3 was used as the fine aggregate material. The weight of the LWAC was reduced by 23–32% compared to that of the normal concrete due to the use of the above three types of lightweight coarse aggregate (see Table 1). The 28-day cubic strength of the LWACs ranged from 19.31 MPa to 48.54 MPa depending on the weight as shown in Table 1, indicating that the use of lighter coarse aggregate resulted to the lower strength. In this paper, the hollow thin-wall steel balls were used as lightweight aggregate material for the preparation of the LWAC mainly on the basis of two considerations: to further reduce the weight of concrete and to keep the advantages of the LWAC as functional material. The lightweight hollow steel ball aggregate can be used as carrier material for a variety of phase-change materials, which can take advantages of the LWAC as functional material such as thermal insulation material. Furthermore, the authors had verified the good thermal insulation properties of the steel ball concrete based on a series of experimental studies. Therefore, beside the investigation of the effect of FRP confinement on the mechanical performance of lighter LWAC, in a sense, this paper has explored the possibility of developing a kind of multi-functional LWAC.

Table 1
Mix proportion and material properties of LWAC.

Groups	Coarse aggregate		Cement (kg/m^3)	Sand (kg/m^3)	W/B	Sand ratio	Dry density (kg/m^3)	ρ_{dl}/ρ_d	Cubic strength (MPa)	Elastic modulus (GPa)
	type	Dose (kg/m^3)								
C1	Class 600 crushed shale ceramsite	383	450	715	0.35	0.40	1659	0.72	26.48	20.21
C2	Class 800 crushed shale ceramsite	607	420	759	0.38	0.42	1776	0.77	48.54	26.80
C3	Sealed steel balls	367	400	729	0.40	0.40	1555	0.68	19.31	22.16

Note: W/B = water to binder ratio; ρ_l = dry density of LWAC; ρ_n = dry density of normal concrete.

(a) Crushed shale ceramsite (b) Hollow sealed thin-wall steel balls

Fig. 1. Appearance of the lightweight coarse aggregates.

Table 2
Comparison of selected properties of the three different lightweight coarse aggregate materials.

Coarse aggregate material	24 h water absorption (%)	Bulk density (kg/m^3)	Apparent density (kg/m^3)	Tube crushing strength (MPa)
Class 600 crushed shale ceramsite	8	528	862	6.4
Class 800 crushed shale ceramsite	6	750	1272	6.4
Sealed thin-wall steel balls	0	504	873	/

Table 3
Specimen details.

Specimen ID	Coarse aggregate material	Number of CFRP layers	Number of samples in each group	Total
C1-0, C1-1, C1-3	Class 600 crushed shale ceramsite	0, 1, 3	3	9
C2-0, C2-1, C2-3	Class 800 crushed shale ceramsite	0, 1, 3	3	9
C3-0, C3-1, C3-3	Sealed thin-wall steel balls	0, 1, 3	3	9

2.1.2. Carbon fiber-reinforced polymers and adhesive

Carbon fiber-reinforced polymers (CFRP) with a nominal thickness of 0.167 mm were used for the confinement of the LWAC. The measured ultimate tensile strength, elastic modulus and the ultimate elongation of the CFRP were 3844.4 MPa, 272.7 GPa and 1.49%, respectively. The adhesive that was applied to wrap the FRP to concrete exhibited an ultimate tensile strength of 55.5 MPa, a compressive strength of 78.4 MPa, a bending strength of 94 MPa, an elastic modulus of 3.215 GPa, and an ultimate elongation at break of 2.2%.

2.2. Test specimens

For the experiments, a total of 27 LWAC columns with a circular cross-section, a diameter of 150 mm and a height of 300 mm were prepared. The columns were grouped and labeled according to the type of lightweight aggregate material used and the number of CFRP layers wrapped around the LWAC columns. The designation of the specimens used in the experiments is explained in detail in Table 3. It should be noted that in Table 3, the test specimens were labeled in the form of Ct-x, with t = 1, 2 and 3, respectively, where t represents the type of coarse aggregate material, i.e., Class 600 crushed shale ceramsite, Class 800 crushed shale ceramsite or sealed steel balls, and x represents the number of FRP layers. For instance, C1-1 represents the LWAC column fabricated from Class 600 crushed shale ceramsite and wrapped with one layer of CFRP.

2.3. Preparation of the test specimens

Imitating the construction method used for the fabrication of FRP confined normal concrete columns, the preparation of the FRP confined LWAC columns consisted of the following steps:

(1) Surface cleaning: Residual foreign material and concrete spalled from the surface of the concrete column substrate were removed using a high-pressure air rifle. Then the concrete column substrate was successively rinsed with clean water and alcohol.
(2) Surface leveling: Holes on the surface of the concrete columns were filled using a cement paste which was allowed to harden.
(3) Wrapping with CFRP sheets: the adhesive was uniformly applied to the surface of the concrete column; the CFRP sheets were dipped into the adhesive and then attached to the surface of the concrete column. A wiper was used to wipe the CFRP sheets and to squeeze out the excessive impregnating adhesive to ensure full contact between the CFRP sheet and the concrete. The splice length of the CFRP at the ends was selected to 150 mm, as shown in Fig. 2(a).
(4) End treatment: To protect the column ends from damage due to stress concentration, both ends of the column were additionally wrapped with two layers of CFRP sheets with a width of 50 mm and a splice length of 150 mm, and the splice of these additional sheets was separated from the splice of the CFRP sheets applied in step (3). The ends of the crushed ceramsite concrete were polished, as shown in Fig. 2(b). For the steel ball concrete, high-strength gypsum was used for leveling to protect the steel balls locally protruding the upper surface (see Fig. 2(c)) from being damaged, as shown Fig. 2(d).

2.4. Test setup and instrumentation

For each FRP-confined LWAC specimen, two axial strain gauges and eight hoop strain gauges were installed at the midheight of the specimens as illustrated in Fig. 3(a), where the character "L" represents the hoop strain gauge used to measure the circumferential deformation of the concrete and the hoop stress acting on the CFRP sheets, and the character "A" represents the axial strain gauge used to measure the axial deformation of the specimen. The hoop strain gauges were evenly distributed around the circumference, with two gauges placed in the overlapping zone. For each unconfined LWAC, three gauges were used to obtain the lateral deformation of the concrete as shown in Fig. 3(b). In addition, two linear variable displacement transducers (LVDTs) were symmetrically installed in the center area of the specimen using an aluminum alloy frame (Fig. 3(c) and (d)), to obtain the axial deformation of the 185-mm midheight region of the specimen.

The test specimens were placed in a 3000 kN microcomputer-controlled electro-hydraulic servo pressure testing machine. Using the displacement control mode, a loading rate of 0.3 mm/min was applied to the columns. The test setup is shown in Fig. 3(c). All the test data, including the loads, strains, and displacements, were recorded simultaneously by a dynamic data logger.

3. Test results and discussion

3.1. Failure modes

3.1.1. Failure mode of the CFRP-confined ceramsite concrete columns

For the plain ceramsite concrete columns, the middle section of ceramsite concrete column was slightly bloated during failure, and many vertical cracks were found on the outer surface of the ceramsite concrete columns, as shown in Fig. 4(a). For the CFRP-confined ceramsite concrete columns, there was no significant change in phenomenon during the initial loading stage of the test. When the load approached the maximum axial force, the fiber in the middle section of the test columns C1-1 and C1-3 produced a "sizzling" noise lasting for a certain period of time. The load was increased until the CFRP in the middle section of the test columns was broken, and the ceramsite concrete in the middle bloated and failed. For the test columns C2-1 and C2-3, a noise associated with brittle rupture was observed when the load was about to reach the maximum axial force, followed immediately by an extremely loud explosive noise when the CFRP in the middle section of the test columns broke, as shown in Fig. 4(b). The images indicate that both the coarse aggregate and the bonding interfaces between the aggregate and the cement paste were damaged simultaneously.

3.1.2. Failure modes of the CFRP-confined steel ball concrete columns

For the plain steel ball concrete columns, cracks were observed shortly after loading was initiated. Because spherical single-grade steel balls were used, the internal sliding of the steel balls induced a recurring eccentric pressure on the plain steel ball concrete columns, resulting in a repeated fluctuation of the readings of the LVDTs on both sides. When a penetrating crack emerged on the outside, the external concrete spalled, and the test columns failed shortly afterwards. After the external concrete spalled, the steel balls fell off as well, as shown in Fig. 5(a). Considering the smooth surface of the steel balls, there was almost no interface adhesion with the cement paste, and the failure of the test columns could be attributed to the interfaces, and no damage occurred to the steel balls.

(a) Wrapping of the LWAC columns with the CFRP sheets

(b) End leveling of the ceramsite concrete

(c) Initial surface of the steel ball concrete

(d) End leveling of the steel ball concrete

Fig. 2. Critical construction steps during the fabrication of the CFRP-wrapped LWAC columns.

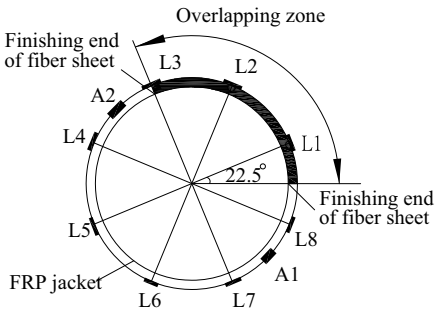

(a) CFRP-wrapped LWAC

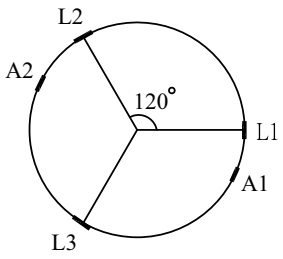

(b) Plain LWAC

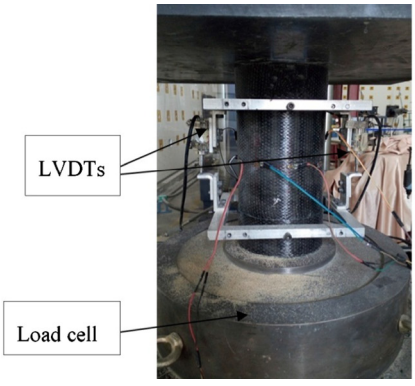

(c) Test setup

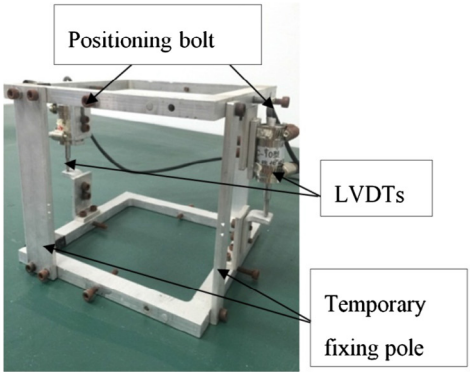

(d) Device used to fixate the LVDTs

Fig. 3. Test setup and instrumentation.

(a) Plain ceramsite concrete column

(b) CFRP-confined ceramsite concrete column

Fig. 4. Failure modes of the ceramsite concrete columns.

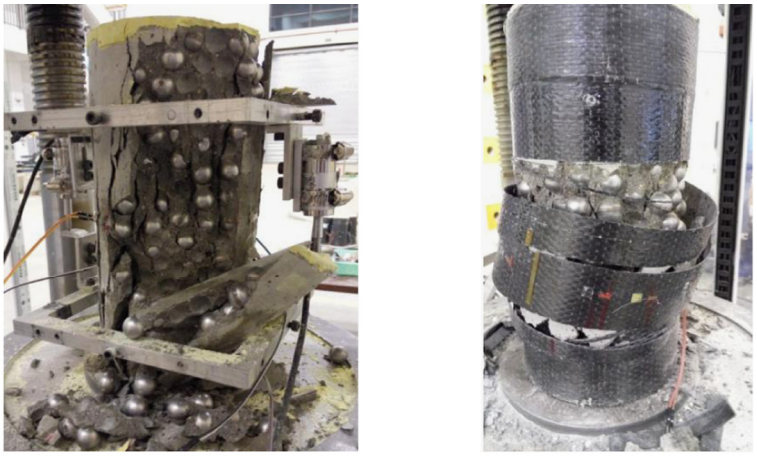

(a) Plain steel ball concrete columns

(b) CFRP-wrapped steel ball concrete columns

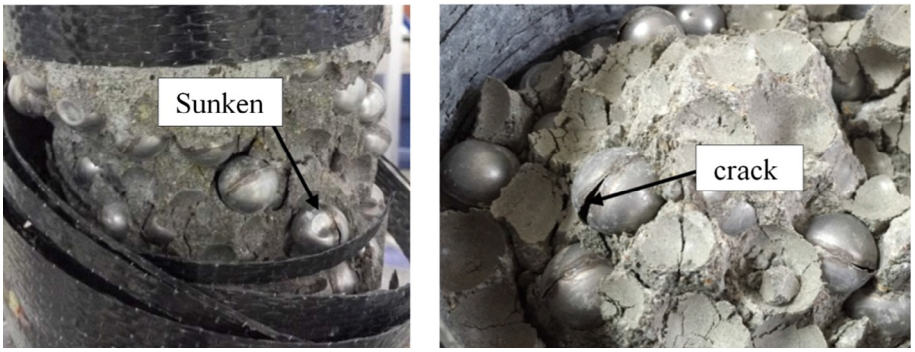

(c) Steel ball sinking phenomena

(d) Rupture of steel balls

Fig. 5. Failure modes of the steel ball concrete columns.

For the CFRP-confined steel ball concrete columns, no significant change in phenomenon was observed during the initial stages of loading. When the load approached the maximum axial force, the CFRP sheets in the middle section of the test columns produced a noise associated with brittle rupture, followed immediately by an extremely loud explosive noise when the CFRP in the middle section of the test columns broke and the test columns failed, as illustrated in Fig. 5(b). The concrete in the middle part of the test columns apparently bloated and cracked, and, in some cases, the test columns split in two, as shown in Fig. 5(b). Most of steel balls in the outermost layer fell off due to the loss of confinement after CFRP rupture. A certain number of steel balls sank due to squeezing after confinement (cp. Fig. 5(c)). Some steel balls in the center of the column cracked and failed around their welding joints (cp. Fig. 5 (d)). As shown in Fig. 5, in comparison to the unconfined concrete, the CFRP confinement had significantly improved the interfacial properties of the steel balls and the cement matrix, maximizing the effect of the mechanical properties of the steel balls.

3.2. General behaviors of the FRP-confined LWAC

The variation of the strength of the CFRP-confined LWAC columns is shown in Table 4 and Fig. 6. After the CFRP confinement, the strength of LWAC columns was found to be significantly improved by a rate related to the strength of the LWAC material and the number of CFRP layers. After wrapping the LWAC columns with one CRFP layer, the strength of the LWAC columns in group C1, C2 and C3 was improved to 1.74, 1.43 and 3.59 times the strength of the plain concrete columns, respectively. After wrapping with three layers of CFRP, the strength of the LWAC columns in group C1, C2 and C3 was improved to 2.60, 2.14 and 5.42 times the strength of the plain concrete columns, respectively. The results also showed that, the lower the strength of the plain LWAC, the higher the increase rate, and the larger the number of CFRP layers, the higher the increase rate. The highest increase was obtained for the steel ball concrete columns which can be explained as follows: The plain steel ball concrete columns were subject to interfacial failure, and the steel balls did not play a significant role. In contrast, in case of CFRP confinement, the interfacial bond properties of the steel balls and the cement matrix were significantly improved, and the strength advantage of steel balls fully applied.

Fig. 7 shows a comparison of the axial stress-strain curves and the hoop expansion stress-strain curves of the LWAC columns as a function of the number of CFRP layers. Under CFRP confinement, the strength and ductility of the LWAC columns were both significantly improved compared with the unconfined LWAC columns. Fig. 7 further reveals that the stress-strain curve obtained for the CFRP-confined LWAC was similar to the curve obtained for the CFRP-confined normal concrete, and could be divided into two distinct segments. The CFRP confinement was not observed to have a significant effect on the stress-strain curve during the initial stage of loading. However, when the applied load exceeded the peak stress value obtained for the corresponding plain concrete, the stress was observed to linearly increase with the strain, and both the strength and ductility of the concrete were found to be significantly improved.

The average ultimate strength and ultimate axial strain of the columns in the C1 group with three layers of CFRP was determined to be 53.97 MPa and 0.036, respectively, corresponding to an increase of the ultimate strain by a factor of 33.4. The ductility of the columns in group C1 was the best compared with the other groups. The highest ultimate strength of 85.31 MPa was obtained for the columns in group C2. For this group, the ultimate axial strain was 0.015, which corresponds to an increase by a factor of 8.5. However, the ductility improvement was the lowest compared with the other groups. The columns in group C3 showed an ultimate strength of 78.36 MPa and an ultimate axial strain of 0.022, corresponding to an improvement by a factor of 31.2. In summary, it can be concluded that the FRP confinement yielded the best improvement in ductility of lower-grade LWAC and the most effective improvement in the strength of higher-grade LWAC. Moreover, wrapping with FRP can be very effective for improving both the strength and ductility of concrete with poor properties of the interface between the aggregate material and the cement matrix, e.g., the steel ball concrete as discussed in this paper.

Fig. 8 shows the hoop rupture strain observed for the CFRP and its distribution along the peripheral direction of the CFRP-confined LWAC during failure. The full-perimeter hoop strain distribution of the CFRP was non-uniform. In all cases, the maximum hoop strain occurred in the non-overlapping zone, which is consistent with the results obtained for the CFRP-confined normal concrete. Similar to the studies on CFRP-confined normal concrete, the ratio of the measured FRP hoop strain/stress ($\varepsilon_{h,rup}/f_{FRP,h}$) at rupture to the ultimate tensile strain/stress (ε_{fu}/f_{FRP}) obtained by flat coupon test was defined as the FRP strain efficiency factor κ_ε, i.e., $\kappa_\varepsilon = f_{FRP,h}/f_{FRP}$ or $\kappa_\varepsilon = \varepsilon_{h,rup}/\varepsilon_{fu}$, which can be used to characterize the effective utilization rate of the FRP material during hoop rupture. The measured CFRP strain efficiency factor is also listed in Table 4. It is seen that the factors obtained for all LWAC columns were roughly the same and were not significantly related to the strength of the LWAC material. In the present paper, the mean value of $\kappa_\varepsilon = 0.53$ was adopted for the analysis before further extensive data are available, which is slightly lower than the strain efficiency factor of 0.586 obtained for CFRP-confined concrete columns [5].

4. Comparison with existing ultimate strength and strain models

Recently, Ozbakkaloglu et al. [29] had reviewed and assessed over 80 existing FRP-confined concrete strength and strain models and it is concluded that of the assessed existing models, the top-performing models for both strength and strain enhancements were determined to be the ones developed by Lam and Teng [5], Jiang and Teng [4], and Ozbakkaloglu and Lim [30]. To provide a quantitative assessment of the differences in behavior between FRP-confined LWAC and FRP-confined normal concrete, the experimental results from the present study are compared with the predictions of the above models. The results are shown in Fig. 9. It can be obviously seen that all of the three best-performing models have significantly underestimated the ultimate strain and none of the three models can have good predictions for the ultimate strength. It may mainly due to the discrepancy in the mechanical properties between the lightweight and the normal aggregates and their interfacial bond behavior with the cement paste. However, it can be seen from Fig. 9(a) that the top-performing strength models can still have good predictions for some test results. An in-depth analysis indicates that these data belong to the specimens with relatively weak confinement ratio. More detailed discussion on this discrepancy is provided in Section 7. Therefore, a new design-oriented model specifically for FRP-confined LWAC is necessary and thus developed in the subsequent section. Its performing is assessed in Fig. 9 as well. The results indicate that the prediction of the proposed model is in close agreement with the test results and can provide improved predictions of the ultimate conditions of FRP-confined LWAC compared to the existing top-performing models.

5. Ultimate strength and strain models for CFRP-confined LWAC

The experimental values obtained for the ultimate strength and strain of the CFRP-confined LWAC are listed in Table 4. Based on

Table 4
Test results of FRP-confined LWAC.

No.	F (kN)	F_m (kN)	f_{co} (MPa)	f_{com} (MPa)	f_{cc} (MPa)	f_{ccm} (MPa)	FRP layers	ε_{co} (%)	ε_{com} (%)	ε_{cc} (%)	ε_{ccm} (%)	ε_h (%)	$\varepsilon_{h,rup}$(%)		κ_ε
													Outside the overlapping zone	Inside the overlapping zone	
C1-0(1)	364	364	20.57	21.18	/	/	0	0.116	0.151	/	/	0.096	/	/	/
C1-0(2)	374		21.18		/			0.094		/		0.158	/	/	/
C1-0(3)	484[a]		27.39[a]		/			-[b]		/		-[b]	/	/	/
C1-1(1)	609	675	/	/	34.46	38.19	1	/	/	0.780	0.886	/	0.717	0.549	0.463
C1-1(2)	675		/		38.19			/		0.875		/	0.418	0.287	0.270[a]
C1-1(3)	883[a]		/		49.98a			/		1.003		/	0.598	0.445	/
C1-3(1)	965	954	/	/	54.58	53.97	3	/	/	3.389	3.502	/	0.701	0.667	0.453
C1-3(2)	933		/		52.78			/		3.475		/	0.769	0.666	0.496
C1-3(3)	964		/		54.54			/		3.641		/	0.787	0.668	0.508
C2-0(1)	722	686	40.86	38.83	/	/	0	0.176	0.180	/	/	0.224	/	/	/
C2-0(2)	471[a]		26.65[a]		/			0.091[a]		/		00157[a]	/	/	/
C2-0(3)	686		38.83		/			0.183		/		0.365	/	/	/
C2-1(1)	1011	1002	/	/	57.21	56.68	1	/	/	0.708	0.669	/	0.756	0.699	0.488
C2-1(2)	992		/		56.16			/		0.631		/	0.814	0.706	0.526
C2-1(3)	1001		/		56.67			/		3.332		/	0.655	0.640	0.423[a]
C2-3(1)	1511	1508	/	/	85.49	85.31	3	/	/	1.506	1.527	/	0.805	0.730	0.520
C2-3(2)	1538		/		87.05			/		1.559		/	0.814	0.718	0.526
C2-3(3)	1474		/		83.39			/		1.516		/	0.885	0.817	0.571
C4-0(1)	238	273	13.47	15.45	/	/	0	0.066	0.0686	/	/	-[b]	/	/	/
C4-0(2)	273		15.45		/			0.071		/		-[b]	/	/	/
C4-0(3)	364[a]		20.60[a]		/			0.150[a]		/		0.0084	/	/	/
C4-1(1)	940	918	/	/	53.17	51.97	1	/	/	1.152	1.268	/	0.867	0.867	0.560
C4-1(2)	934		/		52.85			/		1.410		/	0.898	0.898	0.580
C4-1(3)	881		/		49.88			/		1.242		/	0.778	0.778	0.503
C4-3(1)	1412	1385	/	/	79.89	78.36	3	/	/	2.085	2.141	/	0.948	0.948	0.612
C4-3(2)	1352		/		76.50			/		-[b]		/	-[b]	-[b]	/
C4-3(3)	1391		/		78.70			/		2.198		/	0.925	0.925	0.597

Note: The test columns were labeled in the form of Ct-x (m), where m represents the number of the sample in the group. In Table 4, F = the load-bearing capacity; F_m = the mean load-bearing capacity; f_{co}, f_{cc} = the peak and ultimate strength of concrete, respectively; f_{com}, f_{ccm} = the mean peak and ultimate strength of concrete, respectively; ε_{co}, ε_{cc} = the peak and ultimate strain of concrete, respectively; ε_{com}, ε_{ccm} = the mean peak and ultimate strain of concrete, respectively; ε_h = lateral strain of concrete; $\boldsymbol{\varepsilon_{h,rup}}$ = the CFRP hoop rupture strain. Values denoted by "a" were deemed invalid due to their large deviation, and not considered for the analysis. "-b" indicates that no data could be obtained due to a malfunction of the measuring instrument.

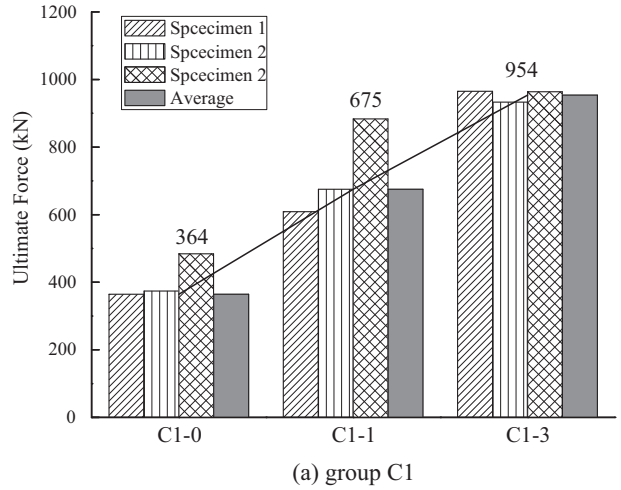

(a) group C1

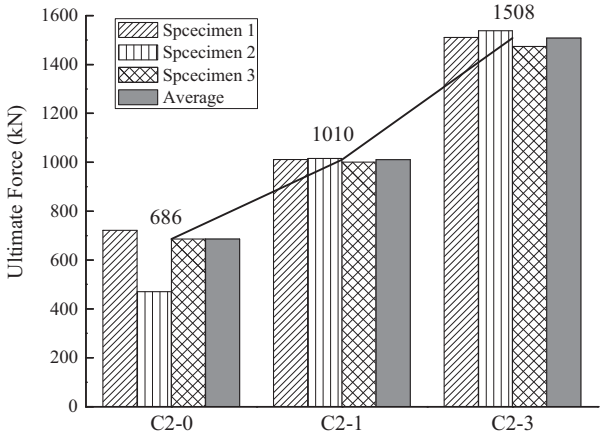

(b) group C2

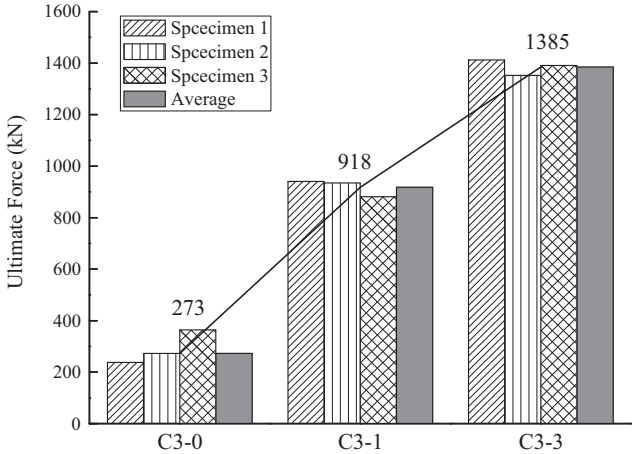

(c) group C3

Fig. 6. The load bearing capacity of the CFRP-confined LWAC columns.

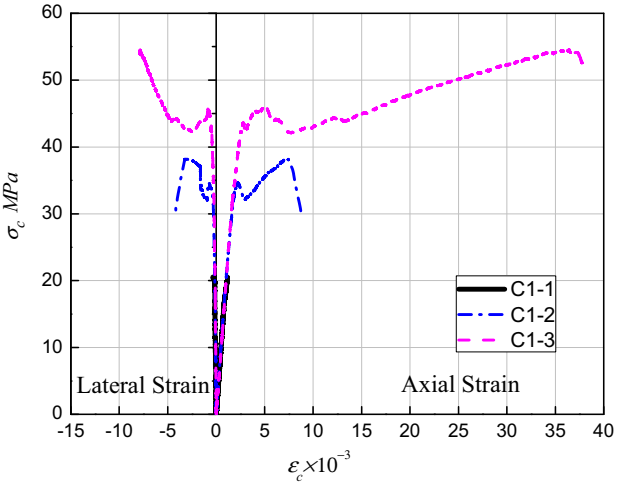

(a) group C1

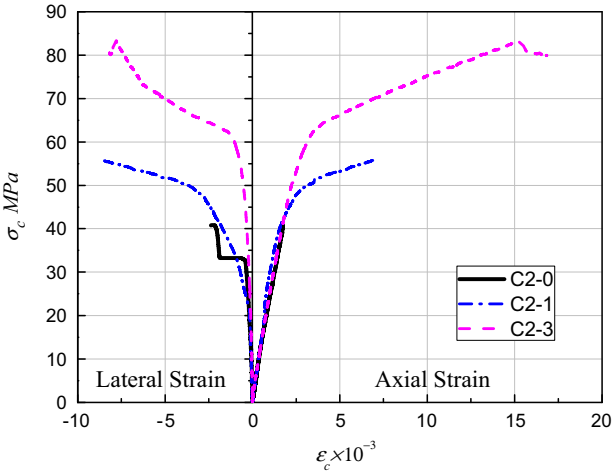

(b) group C2

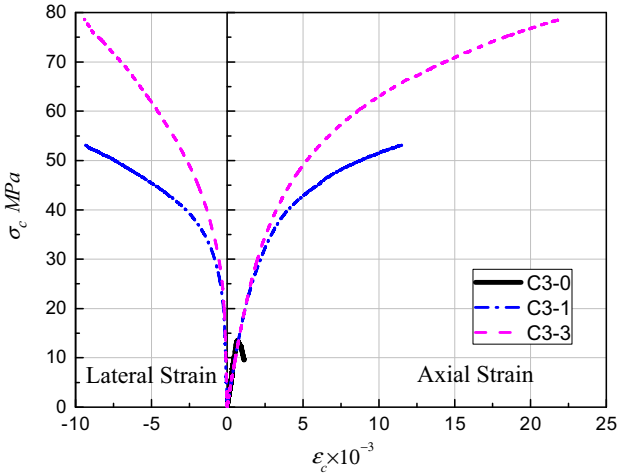

(c) group C3

Fig. 7. Stress-strain curves of FRP confined LWAC.

the experimental results, the ultimate strength and strain models for CFRP-confined LWAC columns are first established this section.

5.1. Ultimate strength model

Ozbakkaloglu et al. [29] had reviewed and assessed over 80 existing FRP-confined concrete models and recommended that the top performing strength enhancement models should be those proposed by Lam and Teng [5], and Teng et al. [8] and etc. Therefore, the following equation form slightly revised from Lam and Teng [5] is proposed to develop the ultimate strength model of CFRP-confined LWAC:

$$\frac{f_{cc}}{f_{co}} = 1 + k_1\left(\eta\frac{f_{le}}{f_{co}}\right)^{k_2} \tag{1}$$

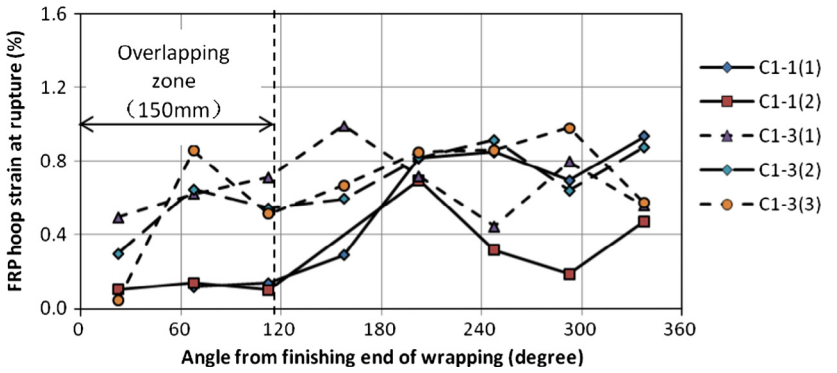

(a) group C1

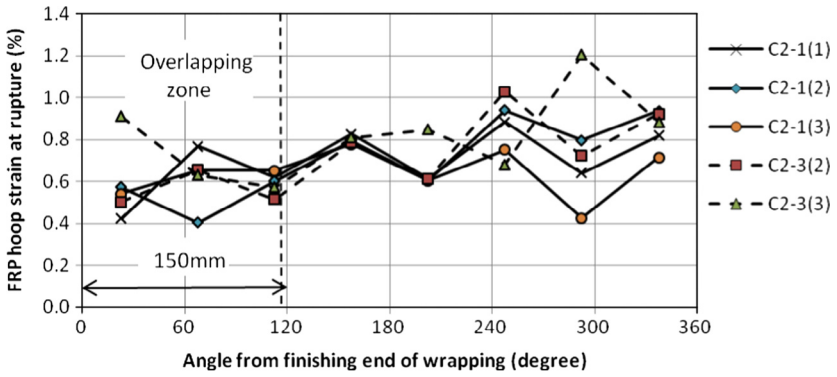

(b) group C2

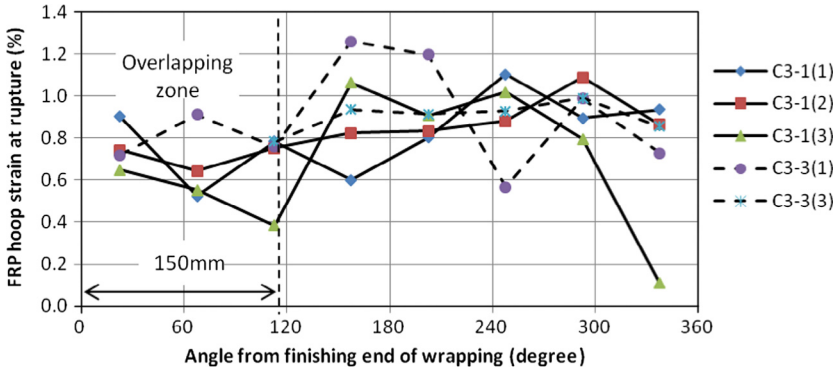

(c) group C3

Fig. 8. Distribution of the CFRP hoop strain at rupture.

where f_{cc} is the ultimate compressive strength of the CFRP-confined LWAC; f_{co} is the ultimate compressive strength of the unconfined LWAC; η is defined as an aggregate type coefficient as the aggregate-cement matrix interfacial bond behavior differs greatly with the change of lightweight aggregate type. As indicated by test previous, the FRP confinement has significantly improved the steel ball aggregate-cement matrix interfacial bond performance but has little effect on the improvement of the crushed ceramsite aggregate-cement matrix interface. Therefore, when crushed ceramsite was used as coarse aggregate material, $\eta = 1$ and when steel balls were used as coarse aggregate material, $\eta > 1$. Furthermore, in Eq. (1), f_{le} is the effective hoop confinement stress, i.e., $f_{le} = \kappa_\varepsilon f_l$ and $f_l = 2\kappa_\varepsilon f_{FRP} t_{FRP}/d$, where f_{FRP} and t_{FRP} represent the ultimate tensile strength and thickness of the CFRP material, respectively, d is the diameter of the column, and κ_ε is the effective CFRP strain efficiency factor, set to $\kappa_\varepsilon = 0.53$.

When using Eq. (1) to fit the test data presented in Table 4, k_1 was determined to 2.11 and k_2 to 0.65. For crushed ceramsite concrete, $\eta = 1.0$, and for steel ball concrete, $\eta = 3.18$, respectively. The fitting correlation coefficient was determined to $R^2 = 0.974$ (see Fig. 10). Therefore, Eq. (1) can be rewritten as:

$$\frac{f_{cc}}{f_{co}} = 1 + 2.11\left(\eta\frac{f_{le}}{f_{co}}\right)^{0.65} \tag{2}$$

Eq. (2) thus gives the strength model for CFRP-confined LWAC.

A comparison of the values predicted using Eq. (2) with the experimental data and the errors is given in Fig. 10. The residual error was calculated by $\omega = \sum|Exp. - Theo.|/\sum|Exp.|$, , where *Exp.* denotes the experimental value and *Theo.* denotes the theoretical value. A residual error of 4.7% was obtained, suggesting that Eq. (2) yields highly accurate results.

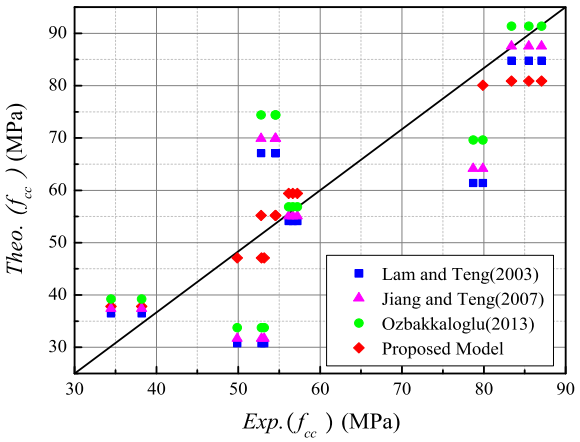

(a) ultimate strength

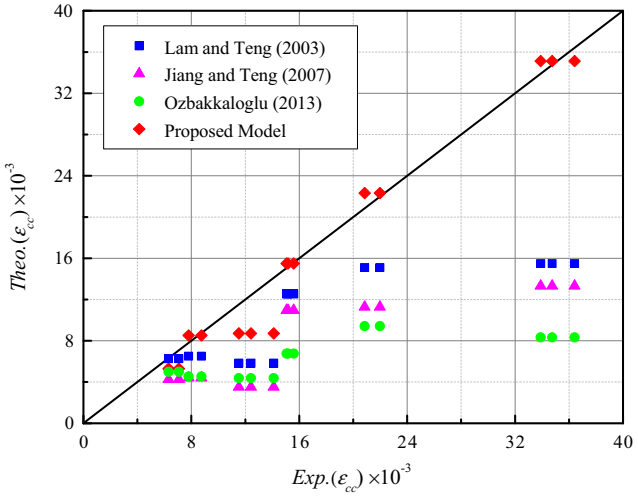

(b) ultimate strain

Fig. 9. Performance of models against the present test results.

5.2. Ultimate strain model

Currently, with regard to the ultimate strain of FRP-confined normal concrete, it is generally assumed that the ultimate strain is related to both the concrete strength and the FRP confinement aspect parameters. Based on the assessment results of over 80 existing FRP-confined concrete models Ozbakkaloglu et al. [29] recommended that the best-performing strain enhancement models were determined to be the ones proposed by Tamuzs et al. [31], Jiang and Teng [4] and Teng et al. [8]. Of the above-mentioned models, Teng et al. [8] had upgraded the understanding on the strain enhancement by firstly introducing two significant parameters with explicit physical meanings, i.e., the FRP confinement stiffness ratio, ρ_k, and the strain ratio, ρ_ε, to develop the ultimate strain model. Therefore, in the present paper, the following formulas are proposed for the calculation of the ultimate strain of FRP-confined LWAC based on Teng et al.'s model [8]:

$$\frac{\varepsilon_{cc}}{\varepsilon_{co}} = c_0 + k_1 \rho_k^{\lambda \cdot k_2} \rho_\varepsilon^{\lambda \cdot k_3} \tag{3}$$

$$\rho_k = \frac{2E_{FRP}t}{(f_{co}/\varepsilon_{co})D} \tag{4}$$

$$\rho_\varepsilon = \frac{\varepsilon_{h.rup}}{\varepsilon_{co}} \tag{5}$$

where ε_{cc} represents the axial ultimate strain of the FRP-confined LWAC; ε_{co} is the strain corresponding to the peak stress of the unconfined LWAC, which is in the range from 0.0020 to 0.0024 according to the *Technical specification for lightweight aggregate concrete structures* (JGJ12-2006) [1]. It should be noted that similarly to the derivation of the ultimate strength model, λ is defined as the aggregate type coefficient that used to quantify the effect of the bond improvement of the steel ball aggregate-cement matrix interface on the ultimate strain of FRP-confined steel ball concrete due to the FRP confinement, that's, when crushed ceramsite was used as coarse aggregate material, $\lambda = 1$ and when steel balls were used as coarse aggregate material, $\lambda > 1$.

With the ultimate compressive strain of unconfined LWAC set to 0.0033 [1], when $f_{le} = 0$, the ultimate strain of plain LWAC is approximately 1.5 times the peak strain, so $c_0 = 1.5$ in Eq. (3).

Using Eq. (3) to fit the experimental data obtained for the ultimate strain, k_1 was determined to 5.24, k_2 to 1.45 and k_3 to 2.63, and $\lambda = 1$ for FRP-confined ceramsite concrete and $\lambda = 0.64$ for FRP-confined steel ball concrete. Therefore, the ultimate strain model is finally obtained:

For FRP-confined ceramsite concrete:

$$\frac{\varepsilon_{cc}}{\varepsilon_{co}} = 1.5 + 5.24\rho_k^{1.45}\rho_\varepsilon^{2.63} \tag{6}$$

For FRP-confined steel ball concrete:

$$\frac{\varepsilon_{cc}}{\varepsilon_{co}} = 1.5 + 5.24\rho_k^{1.45\lambda}\rho_\varepsilon^{2.63\lambda} \tag{7}$$

The accuracy of Eqs. (6) and (7) in predicting the ultimate strain is illustrated in Fig. 11, where the average residual error $\omega = 9.9\%$,

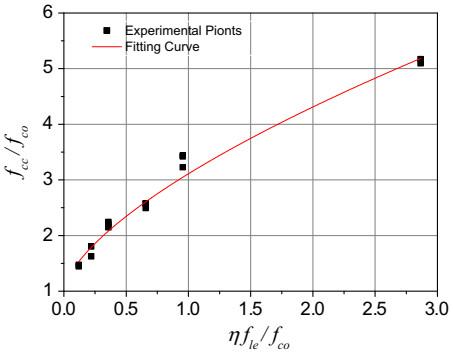

(a) Relation between the ultimate strength and the confinement ratio

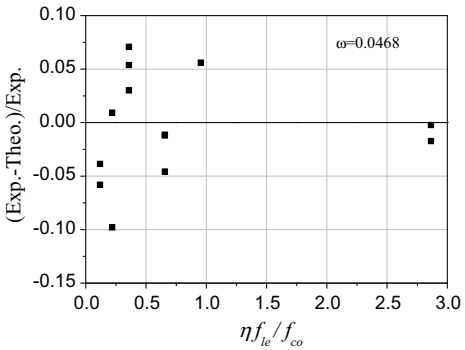

(b) Error analysis

Fig. 10. Values predicted using the ultimate strength model and error analysis.

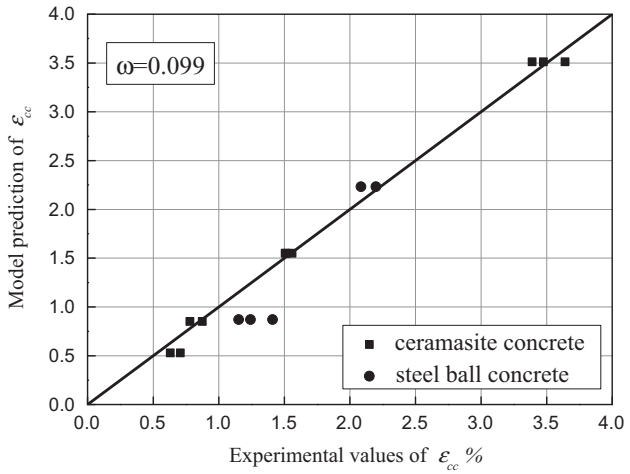

Fig. 11. Error analysis for CFRP-confined light weight concrete.

indicating the relatively high performance of the ultimate strain model.

6. Stress-strain relation models for FRP-confined LWAC

6.1. Stress-strain relationship

The experimental study showed that the stress-strain relation of FRP-confined LWAC was similar to the relation obtained for FRP-confined normal concrete (cp. Fig. 12), which can be clearly be divided into two distinct segments. First, the strength of the FRP-confined LWAC follows a nonlinear trend before reaching the strength of the unconfined concrete, and then linearly increases with the strain. Therefore, the stress-strain relation model for the CFRP-confined LWAC could be established based on the stress-strain relation model for FRP-confined normal concrete. Recently, many scholars proposed several stress-strain relation models for FRP-confined normal concrete columns based on experimental studies and theoretical analysis [5,19–22,10,23–28]. Most of them adopted a single continuous function (parabolic and straight line) [19,21,22,10] or a complex piecewise nonlinear function [5,20,23–25] to describe the stress-strain curve of FRP-confined concrete columns. In the present paper, the model proposed by Zhou and Wu [26] (Eq. (8)) was adopted to establish the stress-strain relation of FRP-confined LWAC. In this model, a single function is used to express a complex bilinear stress-strain relation, which features a simple form and is both integrable and differentiable, and its parameters all have a specific physical meaning (cp. Fig. 12). Moreover, Zhou and Wu's model [26] has been successfully used to develop the stress-strain relation model of FRP-confined load-induced damaged concrete [14,15] recently.

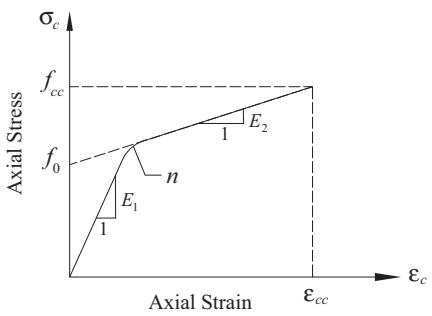

Fig. 12. Stress-strain model proposed by Zhou and Wu.

$$\sigma_c = \left[(E_1\varepsilon_n - f_0)e^{-\frac{\varepsilon_c}{\varepsilon_n}} + f_0 + E_2\varepsilon_c\right]\left(1 - e^{-\frac{\varepsilon_c}{\varepsilon_n}}\right) \quad (8)$$

where σ_c and ε_c are the axial stress and strain of concrete, respectively; f_0 is the stress value at the interception of the asymptotical line with the vertical axis; E_1 is the initial elastic modulus of the stress-strain curve; E_2 is the slope of the asymptotical line of the hardening branch; and $\varepsilon_n = n\varepsilon_0$ where $\varepsilon_0 = f_0/E_1$, and n is the curve shape parameter, controlling the curvature of the transition zone and satisfying $0 < n < 1$, as shown in Fig. 12.

Using Eq. (8) to fit the stress-strain relations of the different FRP-confined LWAC, we could obtain the four model parameters for various confined concrete columns, listed in Table 5. The fitting and the test curves were in good agreement, and the mean value of all fitting correlation coefficients (R^2) was 0.995 (0.997 at maximum and 0.991 at minimum). This suggests that the model proposed by Zhou and Wu yields highly accurate results when used to predict the stress-strain relation of FRP-confined LWAC.

In the following section, the above four model parameters will be determined to establish the stress-strain model of FRP-confined concrete.

6.2. Determination of the model parameters E_1, f_0, n and E_2

6.2.1. Determination of the initial elastic modulus E_1

Being passively confined by the FRP, the concrete showed no significant transverse expansion before the maximum strength of the unconfined concrete was reached. The FRP confinement was weak, so the first curve segment of the stress-strain relation showed a similar trend compared with the unconfined concrete. Thus:

$$E_1 = E_c \quad (9)$$

where E_c represents the initial elastic modulus of the unconfined LWAC.

6.2.2. Determination of f_0

f_0 is a parameter required to determine the bilinear stress-strain curve of FRP-confined LWAC. Based on the works by Samaan et al. [19], the following relationship is suggested to best fit the results of f_0:

$$f_0 = k_1 f_{co} + k_2 m f_{le} + k_3 \quad (10)$$

Table 5
Parameters of the stress-strain model for FRP-confined LWAC.

Specimen ID	f_{le}/f_{co}	f_{cc}/f_{co}'	$\varepsilon_{cc}/\varepsilon_{co}$	f_0 (MPa)	n	E_2 (Mpa)
C1-1(1)	0.219	1.63	6.78	39.750	0.488	-678.205
C1-1(2)	0.219	1.80	7.60	34.595	0.526	410.857
C1-3(1)	0.657	2.58	29.45	42.952	0.456	343.064
C1-3(2)	0.657	2.49	30.19	40.561	0.509	351.583
C1-3(3)	0.657	2.58	31.63	42.178	0.493	339.529
C2-1(1)	0.119	1.47	3.94	50.135	0.455	999.958
C2-1(2)	0.119	1.45	3.52	69.592	0.475	−2128.498
C2-1(3)	0.119	1.46	18.56[a]	–	–	–
C2-3(1)	0.358	2.20	8.39	58.893	0.484	1765.960
C2-3(2)	0.358	2.24	8.68	62.711	0.581	1561.594
C2-3(3)	0.358	2.15	8.45	63.514	0.581	1310.723
C3-1(1)	0.300	3.44	16.79	39.391	0.914	1196.206
C3-1(2)	0.300	3.42	20.56	35.777	0.832	1210.508
C3-1(3)	0.300	3.23	18.11	35.431	0.868	1163.264
C3-3(1)	0.901	5.17	30.39	51.573	1.015	1358.339
C3-3(3)	0.901	5.09	32.04	54.191	1.447	1115.183

Note: Values denoted by "a" value were deemed invalid due to their large deviation, and were not considered for the subsequent analysis. For test column C2-1(3), due to a malfunction of the equipment, the stress-strain curve displayed apparent errors, and the correct data could not be obtained.

where m is the aggregate type coefficient introduced to consider the improvement of the mechanical properties of the steel ball concrete through FRP confinement. Similar to the interface improvement coefficient η or λ introduced in the previous section, it was set to 1.0 when crushed ceramsite was used as coarse aggregate material and >1 when steel balls were used as coarse aggregate material to characterize the effect of the FRP confinement on the improvement of the bond property of the steel ball-cement matrix material interface.

Through regression analyses, k_1 was determined to 1, k_2 to 0.80, and k_3 to 10.7, and m = 1.0 for crushed ceramsite and m = 2.5 for steel ball concrete. Therefore, Eq. (10) can be finally rewritten as:

$$f_0 = f_{co} + 0.8(mf_{le}) + 10.7 \tag{11}$$

A comparison of the predicted values and the experimental data is shown in Fig. 13, where ω = 5.9%.

6.2.3. Determination of n

As shown in Table 5, the value of n did not change significantly, and the mean value n_t was adopted as parameter for the FRP-confined ceramsite concrete, whereas the mean value n_g was adopted as parameter for the CFRP-confined steel ball concrete.

$$n_t = 0.5 \tag{12}$$

$$n_g = 1.0 \tag{13}$$

6.2.4. Determination of E_2

As described above, f_{cc} and ε_{cc} are the ultimate strength and the ultimate strain of FRP-confined concrete, respectively, which represent the effect of the FRP confinement on the strength and ductility of the concrete. Therefore, the slope E_2 of the asymptotical line of the hardening branch of the stress-strain curve was directly obtained via the points (ε_{cc}, f_{cc}) and (0, f_0):

$$E_2 = \frac{f_{cc} - f_{co}}{\varepsilon_{cc}} \tag{14}$$

where f_{cc} and ε_{cc} are obtained using Eqs. (2) and (6)/(7), respectively.

Therefore, the expressions for calculating f_{cc} and ε_{cc} derived in the last section were directly adopted to develop the stress-strain relation model.

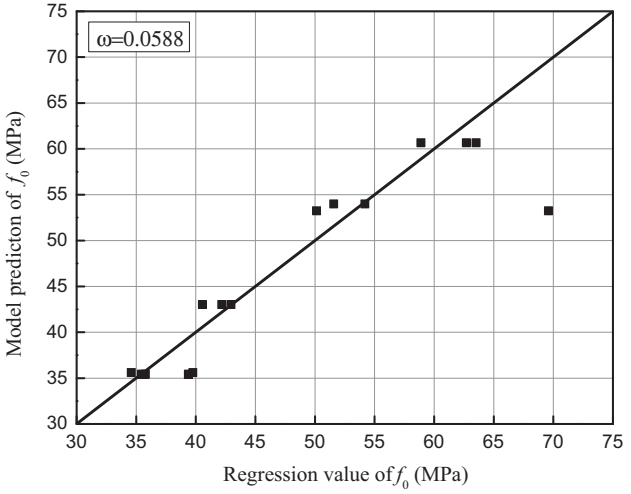

Fig. 13. Error analysis for f_0.

6.3. Experimental verification

Finally, the stress-strain model for the FRP-confined LWAC was established by combining the Eqs. (2), (6)–(9) and (11)–(14). The predicted stress-strain curve and the experimental data are compared in Fig. 14. The results indicate that the stress-strain relation model established for the FRP-confined LWAC was in good agreement with the experimental data, and can be used for an analysis of the mechanical properties of FRP-strengthened LWAC structures.

7. Differences in mechanical behaviors of FRP-confined LWAC and FRP-confined normal concrete

In this section, the differences between FRP-confined LWAC and FRP-confined normal concrete concerning the mechanical properties were further analyzed. Due to the lack of sufficient experimental data for FRP-confined LWAC, the ultimate strength, ultimate strain and stress-strain relation models established in the previous section were used for a comparative analysis with Lam and Teng's model [5] and Teng et al.'s model [8] for FRP-confined normal concrete, as shown in Fig. 15.

Fig. 15(a) reveals the difference between the FRP-confined LWAC and the FRP-confined normal concrete concerning the strength improvement which were evaluated by the proposed and Lam and Teng's [5] models respectively. The results indicate that when the FRP confinement ratio (f_{le}/f_{co}) is below 0.4, the strength improvement observed for the FRP-confined ceramsite concrete is similar to the improvement observed for the FRP-confined normal concrete with the same confinement ratio; and when the FRP confinement ratio (f_{le}/f_{co}) is above 0.4, the strength improvement observed for the FRP-confined ceramsite concrete is lower than the improvement observed for normal concrete. With an increase of the confinement ratio, the differences become more significant. Fig. 15(a) also indicates that the improvement in ultimate strength is the highest for the FRP-confined steel ball concrete, which can be attributed to the fact that the interfacial properties of the steel ball-cement matrix were significantly improved by the FRP confinement, thereby maximizing the effect of the mechanical properties of the steel balls.

Fig. 15(b) reveals the difference between FRP-confined LWAC and FRP-confined normal concrete concerning the ultimate strain which were evaluated by the proposed and Teng et al.'s [8] models respectively. Fig. 15(b) also depicts the effects of the FRP confinement stiffness ratio ρ_k and the strain ratio ρ_ε on the ultimate strain. It can be seen from Eq. (5) that for a certain type of FRP and concrete, the strain ratio ρ_ε is uniquely determined and thus the values of ρ_ε were calculated to be 4.40, 4.37, 6.86 and 11.51 respectively for normal concrete, class 800 (higher-grade) and class 600 (lower-grade) crushed shale ceramsite concrete, and steel ball concrete. Therefore, four different curves corresponding to the three types of LWAC and one type of normal concrete were plotted in Fig. 15(b). The results indicate that the strain ratio ρ_ε has dominating effect on the ultimate strain and the improvement in ultimate strain observed for FRP-confined higher-grade ceramsite concrete is similar to that observed for FRP-confined normal concrete due to the very close value of ρ_ε. However, the enhancement in ultimate strain observed for FRP-confined lower-grade ceramsite concrete is significantly higher than that observed for FRP-confined normal concrete, which suggests that the improvement in ductility due to the FRP confinement is much higher for lower-grade ceramsite concrete compared with normal concrete. The improvement in ductility observed for the steel ball concrete is most significant which can be also attributed to the improvement of the interfacial properties.

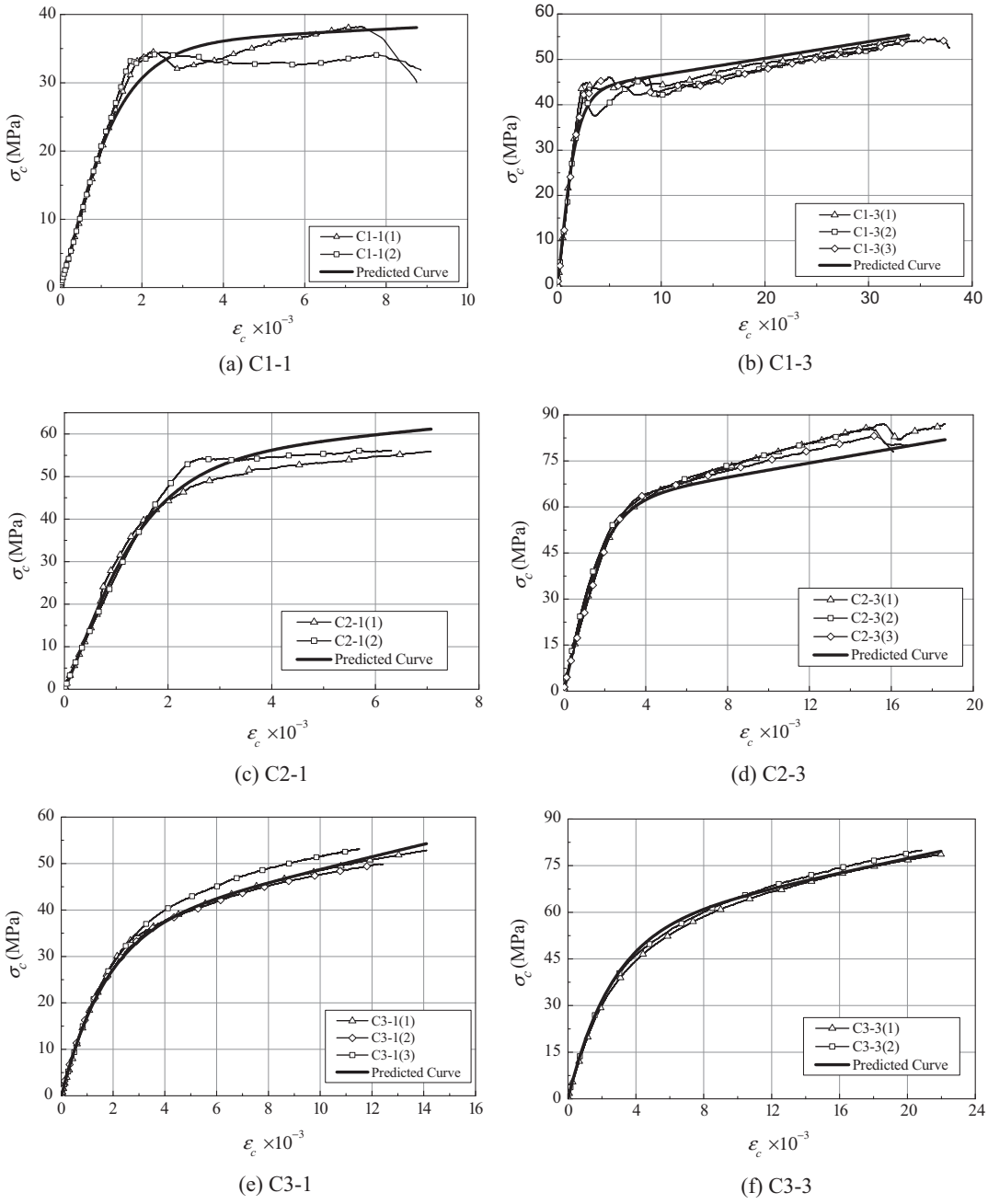

Fig. 14. Comparison of the theoretical and experimental stress-strain curves of CFRP-confined LWAC.

Fig. 15(c) and (d) reveal the differences between the FRP-confined LWAC and the FRP-confined normal concrete concerning the stress-strain relation. Based on the results depicted in Fig. 15 (a) and (b), the difference between the FRP-confined LWAC and the FRP-confined normal concrete concerning the stress-strain relation under two working conditions was analyzed, i.e., a strong CFRP confinement ($f_{le}/f_{co} > 0.4$) and a weak CFRP confinement ($f_{le}/f_{co} < 0.4$). The specimens C1-3 and C2-3 were adopted for a comparative analysis with normal concrete specimens of equivalent strength. Fig. 15(c) shows the stress-strain curves obtained for ceramsite concrete and normal concrete with the same unconfined strength of $f_{co} = 21.18$ MPa wrapped with three layers of CFRP, and the corresponding effective CFRP confinement ratios (f_{le}/f_{co}) were 0.657 and 0.736, respectively, where the difference was due to their different CFRP strain efficiency factor (cp. Eq. (1)). Fig. 15 (c) indicates that, for the same unconfined strength and the same number of CFRP layers, the stress-strain curves obtained for confined ceramsite concrete and normal concrete were almost identical before the peak strength of the corresponding plain concrete was reached. After the stress exceeded the peak strength of the corresponding plain concrete, the confined normal concrete showed a higher stiffness and ultimate strength whereas the confined ceramsite concrete showed a higher ultimate strain. Thus, the CFRP-confined ceramsite concrete showed a superior ductility although at the cost of a relatively low strength. Fig. 15(d) shows the stress-strain curves obtained for ceramsite concrete and normal concrete with the same unconfined strength of $f_{co} = 38.83$ MPa wrapped with three layers of CFRP. The corresponding CFRP confinement ratios (f_{le}/f_{co}) were 0.358 and 0.401, respectively. It can be seen that the two stress-strain curves are similar. The CFRP-confined normal concrete showed a slightly higher stiffness during the second stage, but the ultimate strains were similar, and the dif-

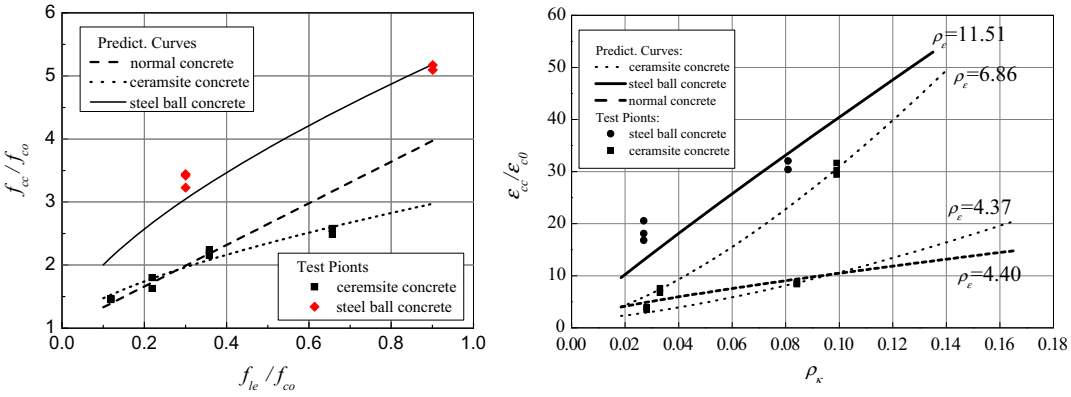

(a) Ultimate strength

(b) Ultimate strain

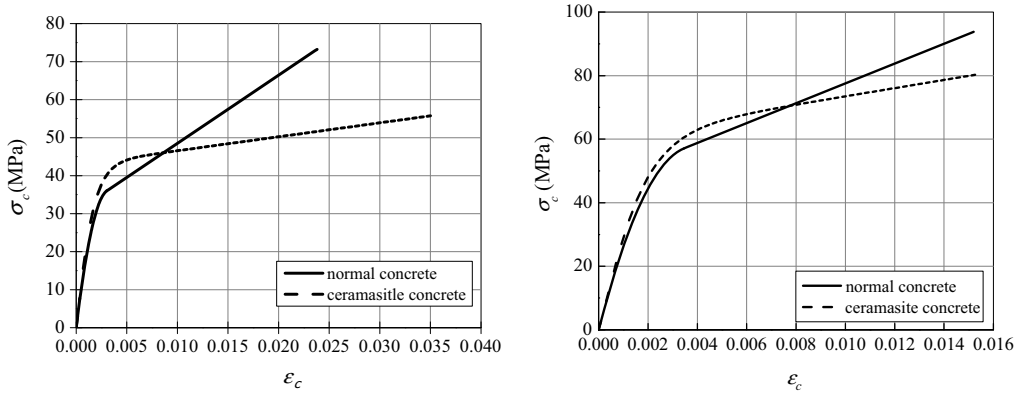

(c) Stress-strain curve in case of relatively strong FRP confinement

(d) Stress-strain curve in case of relatively weak FRP confinement

Fig. 15. Comparison of the mechanical properties of FRP-confined LWAC and FRP-confined normal concrete.

ference in strength was about 15%. Furthermore, the mass of the column could be reduced by roughly 25% when using ceramsite concrete.

8. Conclusions

In the present paper, the mechanical properties of FRP-confined LWAC were experimentally and theoretically studied, and the following conclusions were obtained:

(1) After wrapping with CFRP, the bearing capacity of the LWAC columns was significantly improved, and their ductility was found to be significantly enhanced.
(2) The ultimate strength and ultimate strain models for FRP-confined LWAC were established, and a comparison with the experimental data showed that these models yielded very accurate predictions.
(3) The stress-strain relation model for FRP-confined LWAC was also established. A comparison with the experimental data again showed that the model yielded very accurate predictions.
(4) To realize a low weight and a high-strength of concrete structures and also to explore the possibility of developing a multi-functional LWAC, the possibility of preparing a new lightweight concrete was discussed by using hollow sealed thin-wall steel balls as coarse aggregate material. The mechanical properties of the FRP-confined steel ball concrete were further studied. The experimental results indicated that the strength and ductility of steel ball concrete could be greatly improved by the FRP confinement. Although the hollow sealed thin-wall steel balls do not constitute an ideal alternative aggregate, the results of this study nevertheless indicated that developing a new aggregate material in combination with FRP confinement constitutes an effective approach for the design of a high-strength and lightweight concrete material.
(5) As demonstrated by the comparison of the FRP-confined LWAC and the FRP-confined normal concrete concerning their mechanical properties, when the FRP confinement ratio was lower than 0.4, the improvement of the strength observed for the FRP-confined ceramsite concrete was similar to the improvement observed for the FRP-confined normal concrete. When the FRP confinement ratio was >0.4, the strength improvement observed for the FRP-confined normal concrete was better than the improvement observed for the FRP-confined ceramsite concrete. As for axial deformation, the strain ratio ρ_ε has dominating effect on the ultimate strain and the improvement in ultimate strain observed for FRP-confined higher-grade ceramsite concrete is very close to that observed for FRP-confined normal concrete. However, the enhancement in ultimate strain observed for FRP-confined lower-grade ceramsite concrete and steel ball concrete is significantly higher than that observed for FRP-confined normal concrete, which suggests that the improvement in ductility due to the FRP confinement is much higher for lower-strength LWAC compared with normal concrete.

Acknowledgements

The authors are grateful for the financial support received from the National Natural Science Foundation of China (Grants No. 51378314, 51578338, 51278305), the National Basic Research Program of China (i.e., the 973-project) (Project No. 2011CB013604), and Special Foundation for Overseas High-Caliber Personnel in Shenzhen (Project No. KQCX20140519105054690).

References

[1] JGJ12-2006, Technical Specification for Lightweight Aggregate Concrete Structures, China standard Publishing House, 2006 (in Chinese).
[2] H.T. Wang, L.C. Wang, Experimental study on static and dynamic mechanical properties of steel fiber reinforced lightweight aggregate concrete, Constr. Build. Mater. 38 (2013) 1146–1151.
[3] T.A. Holm, Structural lightweight concrete, in: F.K. Kong et al. (Eds.), Handbook of Structural Concrete, Pitman, London, 1983, pp. 7-1–7-34.
[4] T. Jiang, J.G. Teng, Analysis-oriented stress-strain models for FRP-confined concrete, Eng. Struct. 29 (2007) 2968–2986.
[5] L. Lam, J.G. Teng, Design-oriented stress-strain model for FRP-confined concrete, Constr. Build. Mater. 17 (6–7) (2003) 471–489.
[6] J.G. Dai, Y.L. Bai, J.G. Teng, Behavior and modeling of concrete confined with FRP composites of large deformability, J. Compos. Constr. ASCE 15 (6) (2011) 963–973.
[7] Y.L. Bai, J.G. Dai, J.G. Teng, Cyclic compressive behavior of concrete confined with large rupture strain FRP composites, J. Compos. Constr. ASCE 18 (1) (2014) 04013025.
[8] J.G. Teng, T. Jiang, L. Lam, Y.Z. Luo, Refinement of a design-oriented stress-strain model for FRP-confined concrete, J. Conpos. Constr. 13 (4) (2009) 269–278.
[9] Y.F. Wu, J.F. Jiang, Effective strain of FRP for confined circular concrete columns, Conpos. Struct. 95 (2013) 479–491.
[10] Y. Xiao, H. Wu, Compressive behavior of concrete confined by various types of FRP composite jackets, J. Reinf. Plast. Compos. 22 (13) (2003) 1187–1201.
[11] Y.F. Wu, Y.Y. Wei, Effect of cross-sectional aspect ration on the strength of CFRP-confined rectangular concrete conlumns, Eng. Struct. 32 (1) (2010) 32–45.
[12] J.G. Teng, L. Lam, Compressive behaviour of carbon fiber reinforced polymer-confined concrete in elliptical columns, J. Struct. Eng. 128 (2002) 1535–1543.
[13] Y.F. Wu, Y.W. Zhou, Unified strength model based on Hoek-Brown failure criterion for circular and square concrete columns confined by FRP, J. Compos. Constr. ASCE 14 (2) (2010) 175–184.
[14] Y.F. Wu, Y.C. Yun, Y.Y. Wei, Y.W. Zhou, Effect of predamage on the stress-strain relationship of confined concrete under monotonic loading, J. Struct. Eng. 12 (2000) 139–146.
[15] Y.W. Zhou, X.M. Liu, L.L. Sui, F. Xing, H.J. Zhou, Stress-strain model for fibre reinforced polymer confined load-induced damaged concrete, Mater. Res. Innov. 19 (S6) (2015) 125–131.
[16] Y.W. Zhou, Mali Li, L.L. Sui, F. Xing, Effect of sulfate attack on the stress-strain relationship of FRP-confined concrete, Constr. Build. Mater. 110 (2016) 235–250.
[17] G. Li, Experimental study of FRP confined concrete cylinders, Eng. Struct. 28 (7) (2005) 1001–1008.
[18] A. Mirmiran, M. Shahawy, M. Samaan, H. Echary, Effect of column parameters on FRP-confined concrete, J. Compos. Constr. 2 (4) (1998) 175–185.
[19] M. Samaan, A. Mirmiran, M. Shahawy, Model of concrete confined by fiber composites, J. Struct. Eng. 124 (1998) 1025–1031.
[20] M. Saafi, H.A. Toutanji, Z.J. Li, Behavior of concrete columns confined with fiber reinforced polymer tubes, ACI Mater. 96 (4) (1999) 500–509.
[21] R.M. Richard, B.J. Abbott, Versatile elastic-plastic stress-strain formula, J. Eng. Mech. Div. 101 (4) (1975) 511–515.
[22] D.A. Moran, C.P. Pantelides, Stress-strain model for fiber-reinforced polymer-confined concrete, J. Compos. Constr. 6 (2002) 233–240.
[23] O. Chaallal, M. Shahawy, M. Hassan, Performance of axially loaded short rectangular columns strengthened with carbon fiber-reinforced polymer wrapping, J. Compos. Constr. 7 (2003) 200–208.
[24] G. Wu, Z. Lü, Z. Wu, Strength and ductility of concrete cylinders confined with FRP composites, Constr. Build. Mater. 20 (2006) 134–148.
[25] M.N. Youssef, M.Q. Feng, A.S. Mosallam, Stress–strain model for concrete confined by FRP composites, Compos. Part B: Eng. 38 (2007) 614–628.
[26] Y.W. Zhou, Y.F. Wu, General model for constitutive relationships of concrete and its composites structures, Compos. Struct. 94 (2012) 580–592.
[27] L.A. Bisby, A.J.S. Dent, M.F. Green, Comparison of confinement models for fiber-reinforced polymer-wrapped concrete, ACI Struct. J. 102 (1) (2005) 62–72.
[28] P. Sadeghian, A. Fam, Improved design-oriented confinement models for FRP-wrapped concrete cylinders based on statistical analyses, Eng. Struct. 87 (2015) 162–182.
[29] T. Ozbakkaloglu, J.C. Lim, T. Vincent, FRP-confined concrete in circular sections: review and assessment of stress-strain models, Eng. Struct. 49 (2013) 1068–1088.
[30] T. Ozbakkaloglu, J.C. Lin, Axial compressive behavior of FRP-confined concrete: experimental test database and a new design-oriented model, Compos. Part B 55 (2013) 607–634.
[31] V. Tamuzs, R. Tepfers, E. Zile, O. Ladnova, Behavior of concrete cylinders confined by a carbon composite III: deformability and the ultimate axial strain, Mech. Compos. Mater. 42 (4) (2006) 303–314.